Component Dynamics in Polystyrene/Bis(2-ethylhexyl) Phthalate Solutions by Polarized and Depolarized Light Scattering and Dielectric Spectroscopy

A. K. Rizos*

Department of Chemistry and Foundation for Research & Technology—Hellas, University of Crete, P.O. Box 1527, Heraklion 71409, Greece

R. M. Johnsen and W. Brown

Institute of Physical Chemistry, University of Uppsala, S-751 21 Uppsala, Sweden

K. L. Ngai

Naval Research Laboratory, Washington, D.C. 20375-5320

Received January 23, 1995; Revised Manuscript Received May 10, 1995[⊗]

ABSTRACT: Depolarized Rayleigh, polarized Rayleigh–Brillouin scattering, and dielectric spectroscopy have been used to resolve the dynamics of the two components in concentrated solutions of polystyrene (PS) in bis(2-ethylhexyl)phthalate (DOP) close to and above the glass transition temperature. Two distinct time scales of motion exist in the macroscopically homogeneous PS/DOP solutions which are associated with the faster solvent (DOP) and slower polymer (PS) dynamics with different temperature shift factors. The width and the degree of asymmetry of the distribution of relaxation times determined as a function of temperature for both components increase as temperature decreases, and also as the PS concentration increases, indicating that the contribution at a lower frequency has a larger temperature shift factor, α_T. The temperature dependencies of the most probable relaxation times, τ_i with $i = 1, 2$, of both processes conform to the Vogel–Fulcher–Tammann (VFT) equation. These VFT dependencies for the two components, $i = 1, 2$, in the mixture when replotted respectively against T_{gi}/T, where T_{gi} is the temperature at which $\tau_i(T_{gi}) = 10^0$ s, show a trend that can be expected from the enhancement (mitigation) of constraint dynamics of DOP (PS) with further addition of PS (DOP) to the mixture. There is an exact analogy between the current experimental findings in the mixture of polymer and small-molecule diluent and what we have found in the component dynamics in binary miscible polymer blends. Thus the physics in these two systems are similar. The Rayleigh–Brillouin experiment revealed the existence of an additional faster process associated with a localized motion of the phenyl group of the DOP molecule in the concentrated solutions in agreement with a previously reported study.

Introduction

The dynamics in dense polymer and polymer mixtures have been the subject of intense research efforts recently, mainly because of their fundamental importance. Both translational and rotational dynamics of small molecules and polymers have been studied experimentally and theoretically by a variety of methods[1–10] like polarized and depolarized light scattering (DRS) and molecular dynamics simulations.[11,12] Dielectric spectroscopy (DS),[13,14] oscillatory electric birefringence (OEB),[15] and NMR[16] also revealed in polymer solutions that solvent molecules undergo restricted reorientation in the presence of the polymer. The occurrence of distinct mobilities for each component in polymer blends and polymer solutions has been experimentally observed by ^{13}C NMR,[17] mechanical,[18,19] dielectric,[13,20–24] and dynamic light scattering,[23] and deuteron NMR[25] measurements. However, not until very recently did information on the compositional dependence of the modified component dynamics become available.

In the present paper our objective is to provide experimental measurements of the dynamics of both components in polymer solutions as a function of composition. First, we employ depolarized Rayleigh and polarized Rayleigh–Brillouin scattering to examine the mobility of DOP in solutions of polystyrene (PS) in concentrations that range between 0 and 100% in DOP content. The system is an interesting case where both the solvent and the polymer possess similar optical anisotropies. Thus, the average optical anisotropy per PS monomer is $\langle\gamma^2\rangle/x = 38$ Å^{6}[,26] (where x is the degree of polymerization) and the effective optical anisotropy of DOP is 32 Å.[6,27] Second, depolarized photon correlation measurements (PCS) are used to give in the time domain the broad contribution of the slower (PS) dynamics, whereas the faster solvent (DOP) contribution lies mostly outside the dynamic range of PCS. Third, dielectric spectroscopic measurements are made to complement the PCS data, since the main contribution of the DS relaxation spectra arises from DOP, and hence they help to elucidate the faster DOP dynamics. In the bulk polymer the correlation function of the primary α-relaxation exhibits a broad nonexponential decay. When a low molecular weight solvent like DOP is added to the polymer, the dynamics become considerably more complicated since concentration fluctuations are present together with the reorientational and density fluctuations. These concentration fluctuations give rise to a distribution of local compositions. Concentration flucutations have previously been identified as a mechanism for broadening of the relaxation spectra of polymer blends in the glass transition region.[19,28–31] The current experimental findings are discussed in the framework of the coupling model for homopolymers as it was generalized for polymer blends and polymer/solvent mixtures.[21,22,28,29]

[⊗] Abstract published in *Advance ACS Abstracts,* June 15, 1995.

0024-9297/95/2228-5450$09.00/0

Experimental Section

Samples. Concentrated polystyrene solutions in chromatographic-grade dioctyl phthalate were prepared from carefully dried and vacuum-distilled styrene as previously described[32] by thermal polymerization of the monomer–solvent mixtures at 120 °C for 36 h directly in the measuring cells which were then sealed under vacuum. The conversion of the thermal polymerization was >97%.

Polarized and Depolarized Light Scattering. The polarized and depolarized $I_{VH}(\omega)$ spectra were obtained at a scattering angle of 90° using a piezoelectrically scanned plane Fabry–Perot interferometer (Burleigh RC 110). In the present experiments we have used three different free spectral ranges (FSR) of 22, 12.8, and 5.9 GHz, with a finesse on the order of 70–80. Depolarized (VH geometry) dynamic light scattering measurements were made using the technique and apparatus described earlier equipped with an Ar^+ laser (Coherent Radiation Model Innova 300) emitting vertically polarized light (Glan-Thompson polarizer, extinction better than 10^{-6}) with wavelength 488 nm and an ALV-5000 multibit, multi-τ full digital autocorrelator. The scattered light at angle 90° passed through a Glan-Thompson polarizer with an extinction better than 10^{-7}, whose orientation was adjusted to give the minimum intensity for a dilute solution of high molecular weight polystyrene in ethyl acetate. The detector optics employed a 4-μm-diameter monomodal fiber coupled to the photomultiplier. The index-matching fluid was silicon oil, cooled using a cryostat. Condensation on the cell windows at subzero temperatures was prevented by a N_2 stream playing onto the exposed surfaces.

Inverse Laplace transform (ILT) analysis was carried out using the routine REPES[33] to obtain the corresponding relaxation time distribution. This program is similar to Provencher's CONTIN[34] except that the former directly minimizes the sum of the squared differences between experimental and calculated intensity–intensity $g_2(t)$ correlation functions using nonlinear programming. For a system exhibiting a distribution of relaxation times, the field autocorrelation function $g_1(t)$ (where $g_1^2(t) - 1 = g_2(t)$) is described by a continuous function of the relaxation time τ using the Laplace transform:

$$g_1(t) = \int_0^\infty A(t) \exp(-t/\tau)\, d(\tau) \qquad (1)$$

Relaxation time distributions are given in the form of $\tau A(\tau)$ versus log τ plots, with $\tau A(\tau)$ in arbitrary units. This provides an equal-area representation. Analyses were also made using the Kohlrausch–Williams–Watts (KWW) equation:

$$g_2(t) = \{A \exp[-(t/\tau)^\beta] + B\}^2 \qquad (2)$$

where β ($0 < \beta < 1$) is a fitting parameter describing the shape of the distribution and τ is an average relaxation time. Since a single KWW function is clearly unsuitable to fit the experimental $g_2(t)$ as we show later, the correlation functions were fitted to a double KWW function. This described the broad, slow relaxation for polystyrene with good precision but the fast relaxation due to the solvent less satisfactorily. Failure of the KWW function to fit dielectric and mechanical response of component dynamics in polymer blends has been noted before. After analysis of the correlation curves with GENDIST,[33] a portion of the relaxation distribution may be subtracted in order to simplify the analysis of the remainder. For example, removal of a large slow mode, together with a baseline (if one is detected), could aid in the further analysis of a smaller fast mode. The subtraction procedure is as follows. Since $g_2(t) - 1 = b[g_1(t)]^2$ and $g_1(t) = \{[g_2(t) - 1]/b\}^{1/2}$, one first converts all $g_2(t) - 1$ values to $g_1(t)$. In order to subtract a single relaxation of amplitude A, at relaxation time τ, from the $g_1(t)$ distribution, one subtracts $A \exp(-t/\tau)$ from each of the $g_1(t)$ values. The $g_1(t)$ values are subsequently squared and multiplied by b in order to recover the $g_2(t) - 1$ values. When working with a continuous "distribution", the amplitude referred to above is calculated from the area under a "histogram" bar, that is, the height of the bar times the horizontal distance between points.

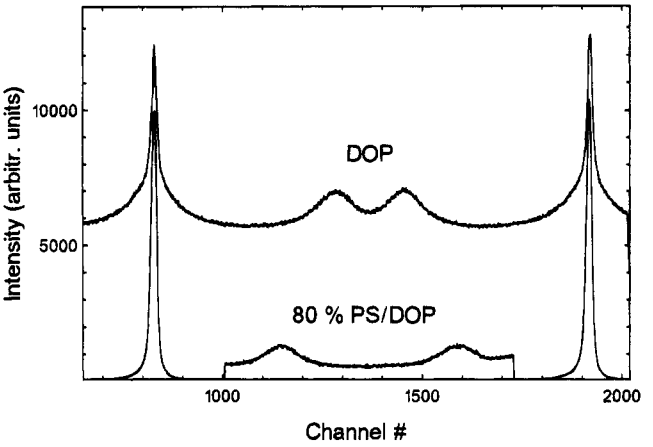

Figure 1. Polarized Rayleigh–Brillouin spectra for neat DOP and a solution of 80% PS/DOP at 353 K.

In our GENDIST program the distance between points is measured as the inverse of the grid density on the log(τ) scale. The fast-decaying portion of the bimodal correlation function was obtained by subtraction of the polystyrene component. This was accomplished by first making an ILT analysis and subsequently deleting the slowly decaying contributions in the data file, following the GENDIST procedure described above. The residual correlation function was then analyzed using a single KWW fit to obtain the solvent relaxation time.

Dielectric Relaxation (DS). The real and imaginary parts of the complex dielectric permittivity ϵ^* were measured from 20 to 10^6 Hz by using a Hewlett-Packard impedance analyzer HP-4284A. The sample was kept between the gold-plated stainless steel electrodes, and the temperature was varied from 203 up to 423 K. The dielectric response originates mainly from the permanent dipole moments in the DOP component of the blend. The experimental $\epsilon''(\omega)$ can be represented by a single Havriliak–Negami (HN) function

$$\epsilon^* - \epsilon_\infty = \Delta\epsilon/[1 + (i\omega\tau_{HN})^\alpha]^\gamma \qquad (3)$$

plus a conductivity term to extract the characteristic relaxation parameters.[35] Here, ϵ_∞ is the high-frequency limiting value of ϵ and α and γ are parameters ($0 \le \alpha$ and $\alpha\gamma \le 1$) describing respectively the symmetric and asymmetric broadening of the distribution of relaxation times.

Results

Polarized Rayleigh–Brillouin Scattering. Polarized Brillouin spectra $I_{VV}(\omega)$ were recorded in the temperature range between 300 and 450 K at a scattering angle of 90°. After repetitive collection, two spectral orders were recorded that consist of two central components and two shifted Brillouin peaks. Figure 1 shows the $I_{VV}(\omega)$ spectra for neat DOP and an 80% PS/DOP solution at 353 K. The two Brillouin peaks are shifted from the incident frequency by $\omega_B = qu(q)$, where q is the wave vector and $u(q)$ is the sound velocity. The linewidth of the Brillouin peaks $\Gamma_B = \alpha u(q)/2\pi$ is related to the attenuation of the sound waves, where α is the attenuation coefficient. It is customary to express the hypersonic loss as $\tan\delta = 2\Gamma_B/f_B$. The Rayleigh–Brillouin spectra display some very interesting features. The shift f_B is intermediate between the corresponding shifts of pure DOP and PS (see Figure 2); however, the linewidth $2\Gamma_B$ is larger than the ones of the pure components. As it is shown in Figure 3a for bulk DOP the Brillouin shift decreases continuously with increasing temperature, whereas the Brillouin linewidth goes through a maximum. Such behavior has been shown to be due to structural relaxation. A characteristic time for the latter is obtained from the frequency at the

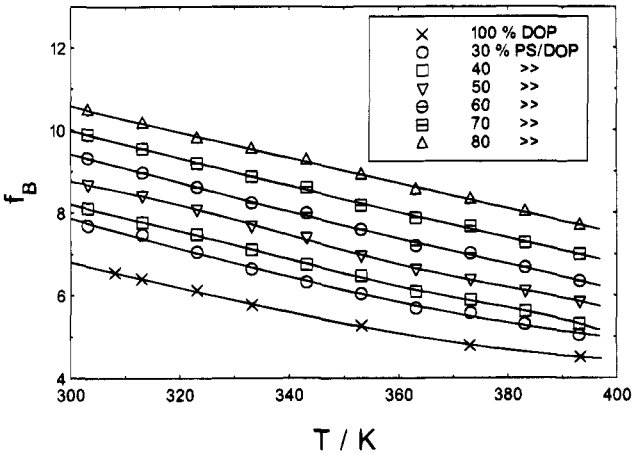

Figure 2. Brillouin shift as a function of temperature at several concentrations.

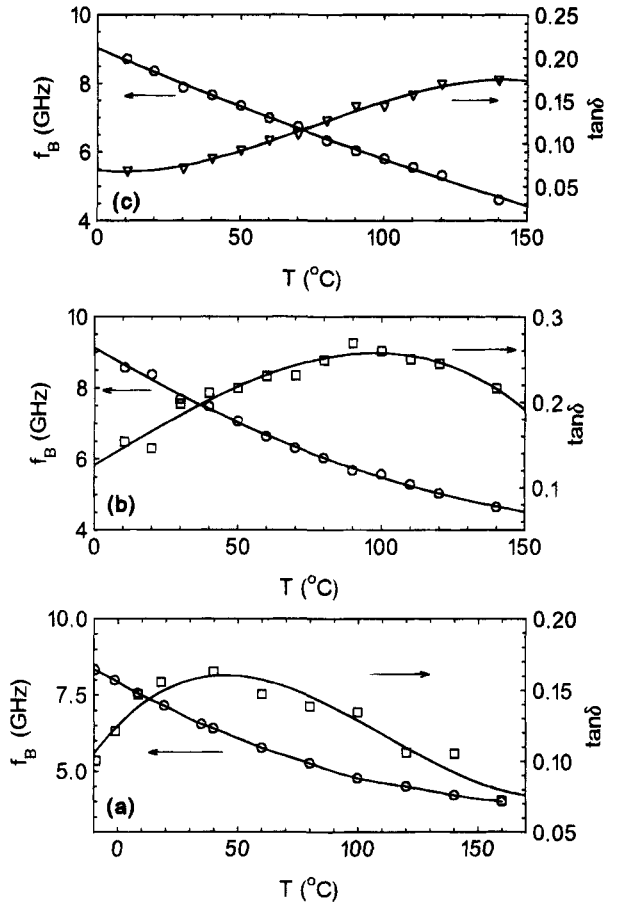

Figure 3. Brillouin shift f_B and hypersonic loss tan δ vs temperature for (a) bulk DOP, (b) a 30% PS/DOP solution, and (c) a 50% PS/DOP solution.

maximum attenuation, i.e., $\tau_{max} = 1/2\pi f_{max}$. Parts b and a of Figure 3 show the evolution of f_B and tan δ with increasing PS concentration. The relaxation times τ_{max}, obtained from the linewidth maximum of the Rayleigh–Brillouin experiments, are very different from the orientational times of the DRS experiments. As was reported previously,[27] this relaxation time reflects a faster motion in the picosecond time scale and is a kind of β-relaxation of the DOP molecule, that could be related to a libration motion of the phenyl ring. Actually, the different values of τ_{max} for bulk DOP (×), 20% PS/DOP (◇), 30% PS/DOP (△), and 50% PS/DOP (⊡),

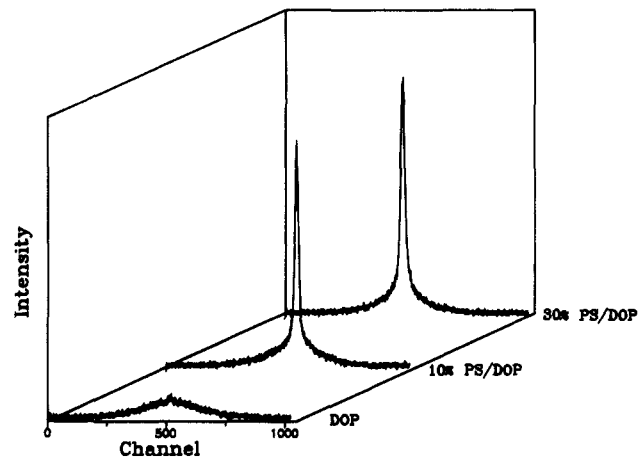

Figure 4. Depolarized Rayleigh spectra of DOP and 10 and 30% PS/DOP solutions at 363 K.

obtained as described above, fall nicely on the same line (see Figure 7), thus implying that this faster relaxation is concentration independent exhibiting a very weak temperature dependence (E = 1.5 kcal/mol).

Depolarized Rayleigh Scattering (DRS). The experimental spectra were described by two Lorentzians plus a baseline:

$$I_{VH}(\omega) = \frac{1}{\pi} I_1 \left[\frac{\Gamma_1}{\Gamma_1 + \omega^2}\right] + \frac{1}{\pi} I_2 \left[\frac{\Gamma_2}{\Gamma_2 + \omega^2}\right] + A \quad (4)$$

where I_1 and I_2 are the integrated intensities of the broad and narrow peaks, Γ_1 and Γ_2 are the corresponding half-widths at half-heights, and A is the baseline. The narrow peak has approximately instrumental width, whereas the width of the broad Lorentzian component is rather insensitive to the FSR's used. The very different reorientational dynamics of the solute and the solvent preserve the selectivity of the technique. Typical depolarized spectra for bulk DOP and for 10 and 30% solutions are shown in Figure 4, whereas in Figure 5 are shown depolarized spectra at three temperatures for a 10% solution in which the broad interferometric component is due to the fast reorienting solvent molecules of DOP, whereas the narrow component is due to the slower polymer dynamics. The difference in the integrated intensities of the narrow and broad peaks is due to the difference in concentration and optical anisotropy of the solute and solvent. The integrated intensity I_{VH} is proportional to the effective optical anisotropy γ_{eff}^2:

$$I_{VH} = Af(n)\, \varrho^* \gamma_{eff}^2 \quad (5)$$

where A is a constant, $f(n)$ is the product of the local field correction and the geometrical factor $1/n^2$, with n being the refractive index, and ϱ^* is the number density of the polymer.

The temperature dependence of the reorientation times of DOP in the mixed systems conform to the Vogel–Fulcher–Tammann (VFT) equation:

$$\log \tau_0 = \log \tau_0^* + \frac{B}{T - T_0} \quad (6)$$

where τ_0^*, B, and T_0 are adjustable parameters.

The influence of the polymer matrix on the solvent dynamics is very limited at high temperatures. Photon correlation spectroscopy (PCS) in the depolarized mode

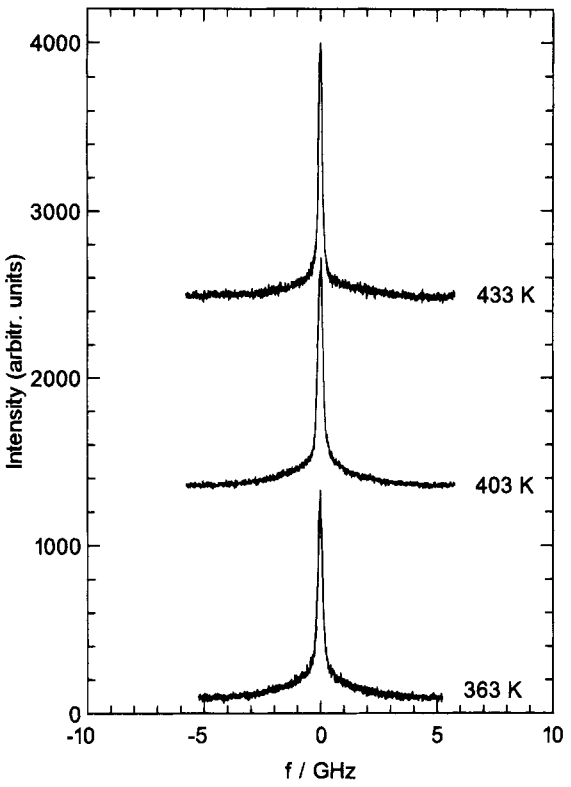

Figure 5. Depolarized Rayleigh spectra of a 10% PS/DOP solution at 363, 403, and 433 K.

has extended the dynamic range to lower frequencies. The depolarized scattered intensity arises from fluctuations in the anisotropic part of the polarizability tensor. The correlation functions $g_{(2)}(t)_{VH}$ were dominated by two relaxation processes. As the solvent fraction increases or the temperature is lowered, the correlation functions are becoming increasingly complex since the relaxation of the solvent enters the time range of PCS. A typical depolarized intensity correlation function is shown in Figure 6 together with its inverse Laplace transform (ILT) using REPES. In order to more clearly present that part of the correlation function due to the solvent relaxation, we show in Figure 6c the residual correlation function obtained after subtraction of the slow part due to the relaxation of polystyrene.

The temperature dependence of the primary relaxation times for the bulk polymer (PS), the neat solvent (DOP), and two of their mixtures is shown in Figure 7. A pertinent feature of Figure 7 is the existence of two non-Arrhenius relaxations. The fast and slow components are due to the solvent and polymer relaxation, respectively. Since the solvent relaxation is only partly present at the limit of the time correlator window, the scatter associated with the fast relaxation times is much greater than that for the slow (PS) component. The VFT parameters for the different concentrations studied are included in Table 1, by combining data from PCS, DRS, and DS. The glass transition temperature T_{gi} for component i in Table 1 is operationally defined as the temperature at which $\tau_i(T_{gi})$ equals an arbitrarily chosen long time of 10^0 s. In Figure 7 it is nicely demonstrated that the dynamics of the present mixed system represent contributions from the α-relaxation of the solvent and polymer components in the mixture, and these can both be followed by DRS at high temperatures and by PCS at lower temperatures. The existence of two distinct time scales of relaxations and different temperature dependencies of the relaxation times of the two

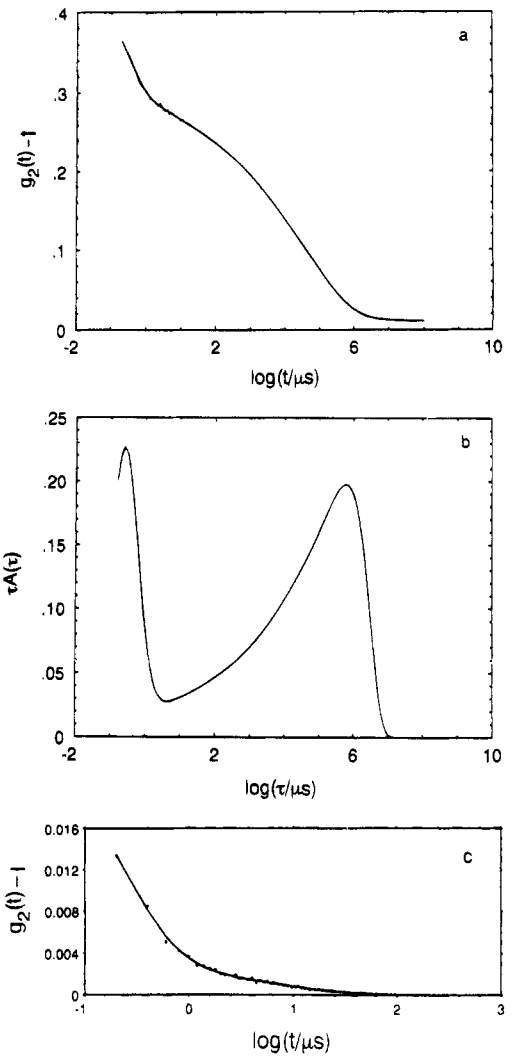

Figure 6. (a) Depolarized intensity correlation function for a 70% PS/DOP mixture at 290 K. (b) Inverse Laplace transform (ILT) of the function in Figure 6a. (c) Residual correlation function after subtraction of the slow part of Figure 6a derived from the relaxation of polystyrene.

Table 1. Vogel–Fulcher Parameters for the Most Probable Relaxation Times of the PS and DOP Components in the Mixtures

	PS component				DOP component			
	log τ_0	B/K	T_0/K	T_g/K	log τ_0	B/K	T_0/K	T_g/K
DOP					−12.05	496	11	184
40% PS/DOP	−12.5	842	178		−12.05	523	159	199
50% PS/DOP	−12.5	886	191	261	−12.05	590	162	212
70% PS/DOP	−12.25	848	219	287	−12.05	598	186	235
PS	−12.5	869	305					

components appears to be a general feature of the dynamics of concentrated polymer solutions.

Dielectric Relaxation. The fast component (due to the neat DOP) in the PCS data which relaxes outside the correlator window can be analyzed using DS. There is a pronounced difference in the relaxation strength between PS and DOP, with the latter having a significantly large dipole moment. Thus in a homogeneous mixture the dielectric response originates mainly from the relaxation of DOP. The dielectric loss curves $\epsilon''(\omega)$ have been described by a single HN function for the different compositions measured, and we are mainly interested in the temperature and concentration dependence of the four parameters that are extracted from the fit, i.e., τ_{HN}, $\Delta\epsilon$, α, and γ.

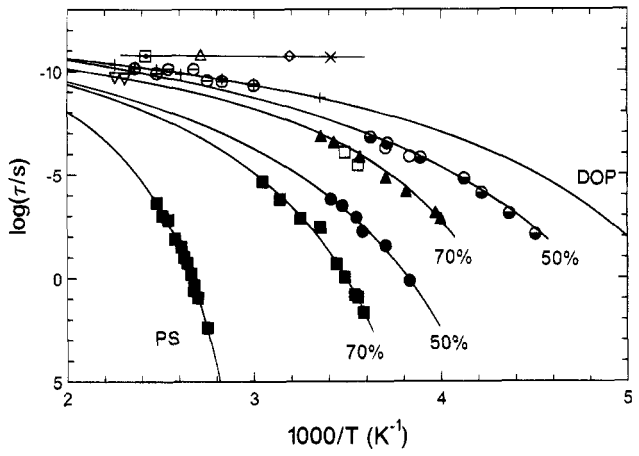

Figure 7. Temperature dependence of the fast (DOP) and slow (PS) relaxation processes in two PS/DOP solutions with concentrations of 50 and 70% PS/DOP. The different values of τ_{max} from the Rayleigh–Brillouin data for bulk DOP (×), 20% PS/DOP (◇), 30% PS/DOP (△), and 50% PS/DOP (⊡) are also included. The relaxation times are also shown by (●,○) PCS, (⊖) DRS, and (◒) DS for the 50% PS/DOP mixture, by (■,□) PCS, (▽) DRS, and (▲) DS for the 70% PS/DOP mixture, and by (+) DRS for pure DOP.

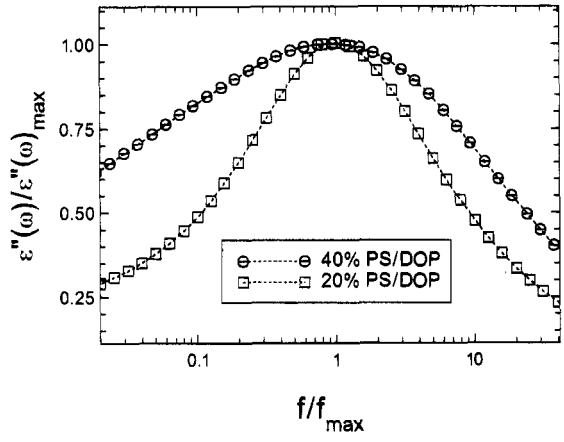

Figure 8. Normalized dielectric loss spectra versus reduced frequency f/f_{max} for the 20 and 40% PS/DOP mixtures at 220 and 235 K, respectively.

In order to compare the data measured with DS in the frequency domain with the results of PCS in the time domain, we have followed a standard procedure[6,36] and transformed the dielectric data in the time domain. The subsequent fit of the dipole moment correlation function to the KWW function gave a temperature- and concentration dependent distribution parameter β. Evidently, the temperature dependence of β is strong, especially for the mixtures. This is in good agreement with the temperature dependence of the HN shape parameters. For the 20% plasticized polymer β changes from 0.6 to 0.8, for the 50% sample β changes from 0.3 to 0.5, whereas for the 70% sample β changes from 0.26 to 0.35 for the low and high temperatures measured. For the 70% sample the distribution parameter β turns out to be the same as that of the unplasticized PS polymer, whereas for the 20% sample the β parameter agrees well with pure DOP. Figure 8 demonstrates the effect of plasticization for the 20 and 40% PS/DOP mixtures. As the PS content increases, the width of the dielectric loss spectra apparently increases. Such very broad dielectric loss spectra with broad distributions of relaxation times that are temperature dependent are expected due to concentration fluctuations. In Figure 7 the data points from DS are in excellent agreement with the data points from the depolarized PCS measurements for the 50 and 70% PS/DOP compositions shown.

Discussion

The results of Fabry–Perot interferometry, depolarized dynamic light scattering, and dielectric measurements on the PS/DOP solutions indicate that from such a combined study the dynamics of each component can be probed. By taking advantage of the small dipolar strength of the PS component, the dielectric measurements selectively observe the dynamics of DOP. The dynamics of the slower component PS in the solutions can be resolved by depolarized dynamic light scattering (PCS). Only the long time tail of the correlation function from the fast DOP component in the mixture appears in the PCS data. In the high-temperature range covered by Fabry–Perot interferometry once again both contributions can be resolved. These measurements, however, monitor the dynamics of the DOP component, since the slow PS contribution is indistinguishable from the instrument resolution. These data covering almost 12 decades provide an opportunity to compare them with the results of the coupling model for miscible polymer solutions and miscible polymer blends.

The discussion to follow on the experimental data of the PS and DOP component dynamics in PS/DOP solutions and the theoretical interpretation by the coupling model will emphasize the close analogy with the component dynamics in miscible binary polymer blends.[20-31] DOP plays the role of PVME in PVME/PS blend[20,21,28] or PIP in PIP/PVE.[24,25,29] The isothermal dielectric loss data for three compositions, 20%, 40%, and 50% PS/DOP shown in Figure 9a–c, serve to illustrate this analogy. It is obvious that concentration fluctuations increase with PS concentration in these three compositions. In addition, the probability that a DOP molecule will see PS monomer units in its neighborhood also increases with PS concentration. Both factors, increasing concentration fluctuation and enriching the various environments of DOP with the presence of PS, broaden the dynamic response of DOP measured here by $\epsilon''(\omega)$. In the coupling model the cooperative dynamics caused by mutual dynamic constraints is governed by the coupling constant, n. An increase in concentration fluctuations gives rise to a broader distribution in local environments in which reorientation of the DOP molecule experiences different dynamic constraints, which in turn engenders a corresponding broader distribution in the coupling parameters, n_α. Each local environment α being richer in PS with an increase in the PS concentration will have the dynamic constraint enhanced and its n_α increased. As has already been explained in the published papers on polymer blends,[21,22,24,28,29] a broader distribution in n_α together with an increase for each n_α leads to strong asymmetric broadening of the ϵ'' peak that is more emphatic on the low-frequency side. Thus we expect that as the PS concentration in PS/DOP, c_{PS}, is increased from 0% to 50%, the loss peak asymmetrically broadens in the manner just described. This expectation is borne out by the dielectric loss data shown in Figure 9. We see that the loss peak becomes progressively broader and more skew asymmetric as c_{PS} increases. It is interesting to point out that the dielectric peak of neat DOP (not shown) is not only narrower

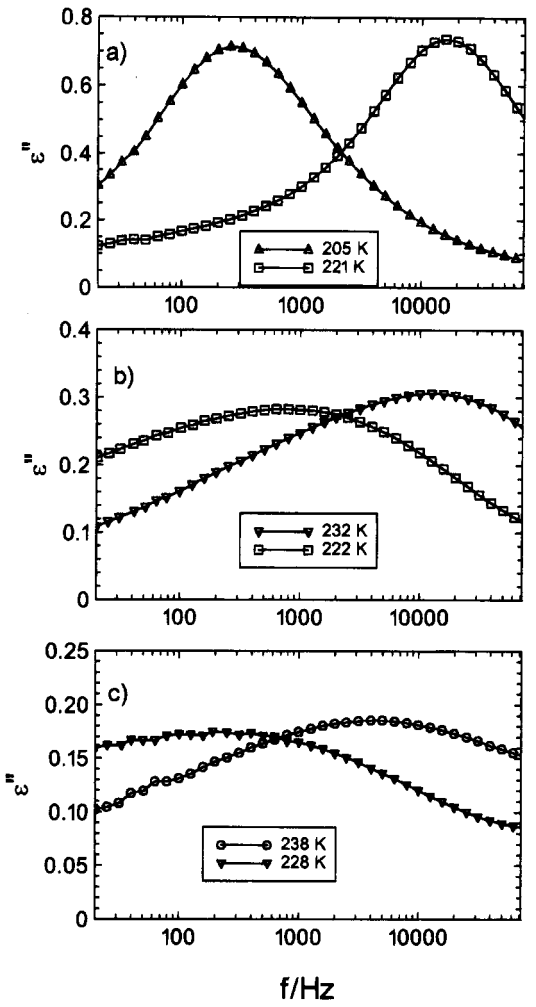

Figure 9. Dielectric loss spectra of (a) 20% PS/DOP, (b) 40% PS/DOP, and (c) 50% PS/DOP.

(though slightly) than that of 20% PS/DOP but also has the opposite skew asymmetry corresponding to the Fourier transform to ϵ'' of the Kohlrausch–Williams–Watts (KWW) stretched exponential function, $\exp[-(t/\tau)^{\beta}]$, which gives a reasonably good fit to the loss peak of neat glass-forming liquids including DOP. The evolution of the peak shape from the KWW skew asymmetry at $c_{PS} = 0\%$ to the almost symmetric form at $c_{PS} = 20\%$ and subsequently to the very broad form with opposite skew asymmetry at $c_{PS} = 40-50\%$ is evident by inspection of Figure 9a–c.

For a fixed composition, say $c_{PS} = 50\%$, different local environments having different n_α's will have correspondingly different temperature shift factors α_{T_α} according to the coupling model.[21,22,28,29] This property is a consequence of the relation between the shift factor and n_α given by:

$$\alpha_{T_\alpha} \propto [\zeta_0(T)]1/(1 - n_\alpha)$$

where $\zeta_0(T)$ is the temperature-dependent friction coefficient before constraint dynamics are incorporated into consideration and should be the same for all environments. From the above consideration it is clear that a larger n_α corresponds to a larger α_{T_i}. This result leads to the prediction that the dynamic response of each component of the PS/DOP mixture is not thermorheologically simple. The dielectric loss peak will change shape because the lower frequency part (that has a larger n_α as discussed above) of the response has a larger α_{T_α}. The degree of this departure from thermorheological simplicity is larger at higher c_{PS} because all the values of n_α in the distribution are larger. This effect is indeed observed in the 40% PS/DOP (Figure 9b) and more clearly in the 50% PS/DOP composition (Figure 9c). The strong broadening toward the low-frequency side is evident by inspection of Figure 9c when temperature is lowered from 238 to 228 K. Similar effects had been observed in the dynamics of the PVME component in the PVME/PS blend by dielectric spectroscopy[20,21,28,31] and of the PIP component in the PIP/PVE blend.[24,25,28,29] These similarities support the interpretation that the lower frequency part of the dielectric loss spectrum is contributed by DOP with an environment that is richer in PS. The degree of thermorheological complexity decreases with decreasing PS content in the mixture as indicated by the data of 20% PS/DOP in Figure 9a. Again this trend is explained by the decrease in the width as well as the average value of the distribution in n_α for the mixture that has a lower PS content. This trend had also been seen in the PIP component dynamics of the PIP/PVE blend from both mechanical and dielectric measurements.[24] At a low concentration of PVE from 15 to 20%, the dynamic response of the PIP component bears a strong resemblance to that of the DOP component in having approximately symmetric, narrower, and close to thermorheologically simple dielectric loss peaks (see Figures 3 and 7 of ref 24). On the other hand, at higher PVE concentration like 50% in PIP/PVE (see Figure 5 of ref 24) or PVME in 50% PVME/PS,[20] very broad and thermorheologically complex loss peaks were obtained respectively for the PIP and the PVME components, analogous to what we observed on the DOP component dynamics in the 50% PS/DOP mixture. In principle, we can carry out a quantitative analysis of the component dynamics of the PS/DOP mixtures at various compositions by using the coupling model as demonstrated before for polymer blends.[21] From the experience gained from ref 37, there is no doubt that the analysis, if carried out, will provide quantitative results of the coupling parameter distributions for the PS and DOP components of the mixture. These results for different compositions will bring out in a quantitative manner the variations of the coupling parameter distribution for each component with PS concentration as we have described qualitatively above. At this time we believe that it is more important to present the experimental data, and a quantitative analysis if necessary can be performed in the future.

To carry out the analogy between the DOP/PS mixtures with the PIP/PVE blends one step further, we shall construct the "cooperativity plots"[24] separately for the DOP and PS components in the same manner as previously done for the PIP and PVE components in the blend.[24] The cooperativity plot is a plot of the most probable relaxation time τ_i of a component i (i = DOP, PS for our present system and i = PIP, PVE for the polymer blend) in a mixture against the normalized reciprocal temperature T_{gi}/T, where the glass transition temperature T_{gi} for component i is operationally defined as the temperature at which $\tau_i(T_{gi})$ equals an arbitrarily chosen long time, say 1 s. The coupling model indicates that the steepness of $\tau_i(T_{gi})$ in the cooperativity plot is proportional to n_i for component i in the local environment that has relaxation time equal to τ_i. Thus in a cooperativity plot for component i in mixtures with different compositions, the variation of steepness with

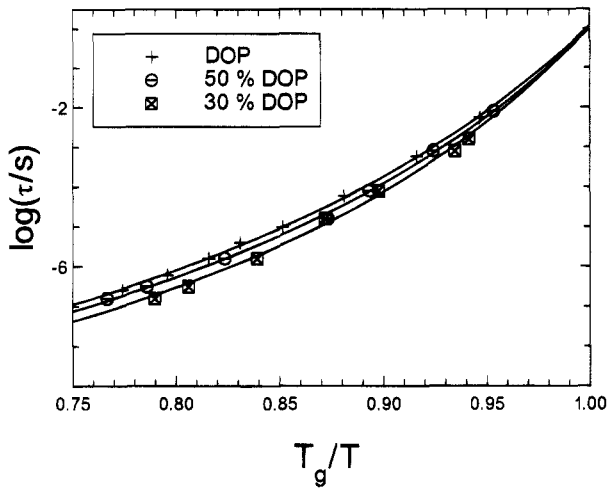

Figure 10. Cooperativity plot for the DOP component in PS/DOP mixtures.

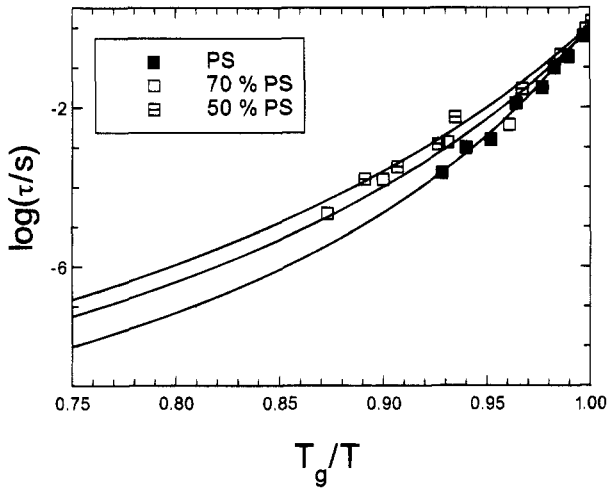

Figure 11. Cooperativity plot for the PS component in PS/DOP mixtures.

composition should follow that of n_i in a predictable manner according to the coupling model as discussed earlier for polymer blends and in the paragraphs above. The experimental data of the PIP/PVE (see Figures 13 and 14 of ref 24) and PVME/PS (see Figure 3 of ref 21) blends are in perfect agreement with the predictable trend of variation of the steepness with composition change. Let us construct also the cooperativity plot for both the DOP and the PS components in our mixtures. We have chosen $\tau_i(T_{gi}) = 1$ s to minimize the error of extrapolation of data taken at shorter times by the Vogel–Fulcher fits with parameters shown in Table 1. Cooperativity plots for DOP and separately for PS constructed from the data and the Vogel–Fulcher fits are shown in Figures 10 and 11, respectively. Figure 10 for the DOP component indicates a monotonic increase of steepness with concentration of PS, consistent with the expected corresponding increase of n_{DOP}. The size of the increase in steepness is comparable to that seen for the PIP component in the PIP/PVE blends. On the other hand, Figure 11 shows the steepness of the PS component continues to decrease with decreasing PS concentration, consistent with the expected corresponding decrease of n_{PS}. Again the effect is similar to that experienced by the PVE component in the PIP/PVE blends.

The ostensively good correspondence between the DOP and the PS component dynamics in our PS/DOP mixtures with the polymer component dynamics in binary polymer blends leads naturally to the conclusion that the physics of the dynamics of DOP/PS mixtures and of binary miscible polymer blends must be quite similar. Moreover, the component dynamics of both systems can be well described by the coupling theory. The existence of two relaxation processes with different VFT equations on a homogeneous mixture is perhaps no surprise when the components are glass formers with widely different T_g's. Moreover, the facts that (1) time–temperature superposition can fail both in miscible polymer blends and solutions and (2) the underlying phenomenon is the same in both systems may have been anticipated by other works in the past. Nevertheless, to the best of our knowledge, the data presented in this work are the first in being able to resolve the dynamics (both dispersion at isothermal condition and temperature evolution) of the two components in a mixture of polymer with a small-molecule glass former. Details of the component dynamics, including the asymmetric broadening of the isothermal relaxation spectrum of the lower T_g component (DOP), particularly on the low-frequency side, are obtained from this work that can be used to compare with the corresponding features seen in polymer blends. In this sense there is new information gained through the experimental part of this work.

The successful comparison of the coupling theory with experimental data has been carried out using predictions of the theory, most of which are not counterintuitive. Although, the trends predicted for the cooperativity plots (see Figures 10 and 11) which are in agreement with experimental data are not expected intuitively. Thus, the data on PS/DOP mixtures presented here alone cannot convincingly verify the unique applicability of the coupling theory. However, in another polymer/solvent system where the polymer is poly(methylphenylsiloxane) (PMPS) with $M_W = 120\,000$ and the solvent is 1,1-bis(*p*-methoxyphenyl)cyclohexane (BMC), there is something counterintuitive happening.[13][37,38] Since the PMPS has a higher glass transition temperature than BMC, its addition might be expected to slow down BMC reorientation, like PS does to DOP in this work. On the contrary, however, at all temperatures the BMC relaxation time is observed to decrease upon addition of 10% PMPS.[37,38] Nevertheless, this counterintuitive observation can be explained by the coupling model.[37,38] At present, besides the coupling theory, there is only an additional theory for component local segmental dynamics of polymer blends by Fischer and Zetsche.[31] We would like to see other different approaches of glass transition dynamics in blends and mixtures which will stimulate research in this field.

Conclusion

In the present work we have examined the solvent (DOP) and polymer (PS) orientation dynamics in concentrated solutions of PS/DOP for polymer concentrations ranging between 10 and 90% using polarized Rayleigh–Brillouin, depolarized Rayleigh scattering, and dielectric spectroscopy. Although macroscopically homogeneous, two distinct time scales are present in the PS/DOP solutions, which are associated with fast and slow relaxation processes exhibiting different Vogel–Fulcher–Tammann temperature dependencies. Moreover, there is significant asymmetry broadening in the distribution of relaxation times for both components PS and DOP due to local composition fluctuations. The

properties of the component dynamics seen in our PS/DOP mixtures are very similar to those of the component dynamics found previously in miscible polymer blends and can be well described by the coupling model.

Acknowledgment. This work is supported in part (W.B. and R.M.J.) by the Swedish Natural Science Research Council (NFR).

References and Notes

(1) Quano, A. C.; Pecora, R. *Macromolecules* **1980**, *13*, 1167.
(2) Oliver, N. H.; Pecora, R.; Quano, A. C. *Macromolecules* **1985**, *18*, 2208.
(3) Fytas, G.; Fizos, A.; Floudas, G.; Lodge, T. P. *J. Chem. Phys.* **1990**, *93*, 5096.
(4) Floudas, G.; Fytas, G.; Brown, W. *J. Chem. Phys.* **1992**, *96*, 2164.
(5) Floudas, G.; Steffen, W.; Fytas, G. *J. Phys. C* **1990**, *2*, 307.
(6) Rizos, A.; Fytas, G.; Lodge, T. P.; Ngai, K. L. *J. Chem. Phys.* **1991**, *95*, 2980.
(7) Floudas, G.; Steffen, W.; Giebel, L.; Fytas, G. *Prog. Colloid Polym. Sci.* **1993**, *91*, 124.
(8) Floudas, G. Ph.D. Thesis, University of Crete, Heraklion, Greece, 1992.
(9) Floudas, G. *J. Non-Cryst. Solids* **1994**, *172–174*, 729.
(10) Brown, W.; Nicolai, T. *Macromolecules* **1994**, *27*, 2470.
(11) Takeuchi, H.; Roe, R. J.; Mark, J. E. *J. Chem. Phys.* **1990**, *93*, 9042.
(12) Muller-Plathe, F. *J. Chem. Phys.* **1991**, *94*, 3192. Kim, E.-G.; Mattice, W. L. *J. Chem. Phys.* **1994**, *101*, 6242.
(13) Hains, P. J.; Williams, G. *Polymer* **1975**, *16*, 725.
(14) Adachi, K.; Ishida, Y. *J. Polym. Sci., Polym. Phys. Ed.* **1976**, *14*, 2219.
(15) Morris, R. L.; Amelar, S.; Lodge, T. P. *J. Chem. Phys.* **1988**, *89*, 6523.
(16) Gisser, D. J.; Ediger, M. D. *Macromolecules* **1992**, *25*, 1284.
(17) Roland, C. M.; Lee, G. F. *Rubber Chem. Technol.* **1988**, *63*, 554.
(18) McCrum, N. G.; Read, B. E.; Williams, G. *Anelastic and Dielectric Effects in Polymeric Solids*; John Wiley: New York, 1967; p 434.
(19) Miller, J. B.; McGrath, K. J.; Roland, C. M.; Trask, C. A.; Garroway, A. N. *Macromolecules* **1990**, *23*, 4543.
(20) Zetsche, A.; Kremer, F.; Jung, W.; Schulze, H. *Polymer* **1990**, *31*, 1883.
(21) Roland, C. M.; Ngai, K. L. *Macromolecules* **1992**, *25*, 363.
(22) Ngai, K. L.; Roland, C. M.; O'Reilly, J. M.; Sedita, J. S. *Macromolecules* **1992**, *25*, 3906.
(23) Fytas, G.; Rizos, A. K.; Alig, I.; Kremer, F.; Roovers, J. *Polymer* **1993**, *34*, 2263.
(24) Alegria, A.; Colmenero, J.; Ngai, K. L.; Roland, C. M. *Macromolecules* **1994**, *27*, 4486.
(25) (a) Chung, G.-C.; Kornfield, J. A.; Smith, S. *Macromolecules* **1994**, *27*, 964. (b) Chung, G.-C.; Kornfield, J. A.; Smith, S. *Macromolecules* **1994**, *27*, 5729.
(26) Floudas, G.; Fytas, G.; Momper, B.; Saiz, E. *Macromolecules* **1990**, *23*, 498.
(27) Floudas, G.; Higgins, J. S.; Fytas, G. *J. Chem. Phys.* **1992**, *96*, 7670.
(28) Roland, C. M.; Ngai, K. L. *J. Rheol.* **1992**, *36*, 1691.
(29) Roland, C. M.; Ngai, K. L. *Macromolecules* **1991**, *24*, 2261.
(30) Shears, M. F.; Williams, G. *J. Chem. Soc., Faraday Trans. 2* **1973**, *69*, 608.
(31) Fischer, E. W.; Zetsche, A. *Polym. Prepr. (Am. Chem. Soc., Div. Polym. Chem.)* **1992**, *33*, 78.
(32) Brown, W.; Johnsen, R. M.; Konak, C.; Dvoranek, L. *J. Chem. Phys.* **1991**, *95*, 8568.
(33) Jakes, J. *Czech. J. Phys. B* **1988**, *38*, 1305.
(34) Provencher, S. W. *Makromol. Chem.* **1979**, *180*, 201.
(35) Havriliak, S.; Negami, S. *Polymer* **1967**, *8*, 101.
(36) Boese, D.; Momper, B.; Meier, G.; Kremer, F.; Hagenah, J.-U.; Fischer, E. W. *Macromolecules* **1989**, *22*, 4416.
(37) Santagelo, P. G.; Roland, C. M.; Ngai, K. L.; Meier, G. *Macromolecules* **1994**, *26*, 6164.
(38) Santagelo, P. G.; Roland, C. M.; Ngai, K. L.; Rizos, A. K.; Katerinopoulos, H. *J. Non-Cryst. Solids* **1994**, *172–174*, 1084.

MA950083H